LA-7891-MS
Informal Report



# Tomographic Visualization of Stress Corrosion Cracks in Tubing





LOS ALAMOS SCIENTIFIC LABORATORY
Post Office Box 1663 Los Alamos, New Mexico 87545

LA-7891-MS
Informal Report
UC-78
Issued: June 1979

# Tomographic Visualization of Stress Corrosion Cracks in Tubing

R. A. Morris
R. P. Kruger
G. W. Wecksung



# TOMOGRAPHIC VISUALIZATION OF STRESS CORROSION CRACKS IN TUBING

by

R. A. Morris

R. P. Kruger

G. W. Wecksung

ABSTRACT

A feasibility study was conducted to determine the possibility of detecting and sizing cracks in reactor cooling water tubes using tomographic techniques. Due to time and financial constraints, only one tomographic reconstruction using the best technique available was made. The results indicate that tomographic reconstructions can, in fact, detect cracks in the tubing and might possibly be capable of measuring the depth of the cracks. Limits of detectability and sensitivity have not been determined but should be investigated in any future work.

---

## 1. INTRODUCTION

The basic goal was to demonstrate the feasibility of visualizing radial cracks caused by stress corrosion in reactor cooling tubes by computed tomographic reconstruction. The tomographic results will in turn, be used by the Battelle Northwest Laboratory to calibrate an eddy current inspection for the tubing.

The cracks occur on the outside diameter of the nominal 1.2-mm thick wall tube and generally run with the tube axis in the plane of the crack. The cracks vary in depth and width, but are all less than 0.1-mm wide and have a maximum depth equal to the wall thickness (1.2 mm). The outside diameter of the tubing is 22 mm.

In general, radiography or radiation transmission gauges are not the inspection of choice when tight cracks are to be detected because the sensitivity of any radiographic technique to cracks is a very sensitive function of crack orientation. In fact this reasoning is implicit in the choice of eddy currents as the primary inspection technique for stress corrosion cracks. However, quantitative sizing of defects

is very difficult if not impossible with eddy currents if good standards are not available. In principle, eddy current testing with more than one frequency has the capability of measuring defect size but the theoretical understanding of the problem is not advanced enough to solve this problem without standards. Tomography, while basically a radiation gauging technique and hence relatively insensitive to cracks, does yield a result that sizes defects to within the accuracy implied by the sampling theorem. The appendix describes the basic principles of tomography as it was applied to this problem.

## II. PROCEDURE

Because the features to be visualized are very small (< 0.1 mm x 1 mm) with high x-ray absorbtion contrast, industrial x-ray film was chosen as the detector. While the film has relatively low dynamic range, it has excellent spatial resolution comparable to a collimated nuclear detector. Figure 1 illustrates the equipment. The 4-mm radiation gap projects to 4.7 mm on the film. This requires that the film translate 5.7 mm between exposures to prevent double exposures. The x-ray source was shielded with lead bricks with a small port to collimate or at least minimize the stray scattered radiation. This problem will be discussed later. Table 1 lists the radiographraphic exposure data.

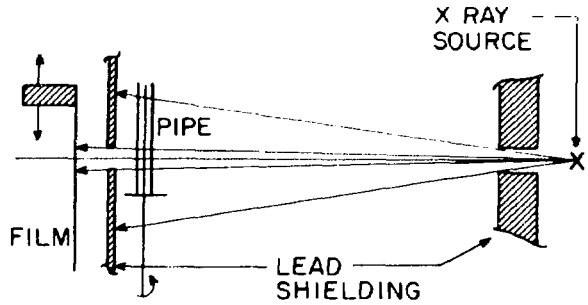

Fig. 1. Tomographic geometry.

Table 1

Radiographic Exposure Data

| | |
|---|---|
| Energy/mA | 200kV/4mA |
| Exposure time | 2 minutes |
| Film load | Eastman Kodak Type M with 0.1 mm Pb screens |
| Target-film-distance | 145 cm |
| Target-slit-distance | 125 cm |
| Target-object-distance | 119 cm |

After each exposure, the tube was rotated 1 degree and the film advanced 5.7 mm. Because the exposure slit plates were relatively thin, the background radiation started building up which limited each film to 20 exposures. The fiducial plate was mounted on the back of the upper exposure slit plate and served as a reference mark for the subsequent microdensitometer scanning. To permit the fan-beam geometry to be corrected to the normal parallel beam geometry, views were taken from -10 to 190 degrees.

After the films were developed, each slit image was scanned with a scanning microdensitometer using a 100 μm X 1500 μm slit. The 100 μm dimension was parallel to the scanning direction. The digital data resulting from each scan was stored on magnetic tape prior to manipulation in the computer. The scans were aligned by referencing the start of each scan to the fixed fiducial image.

The first tomographic reconstruction revealed two potentially serious sources of error.

1. The background radiation had built up after the 20 exposures to produce a nonuniform background.
2. The alignment of slit, object, and axis of rotation left something to be desired. In particular, the exact location of the axis of rotation was unknown.

In an effort to minimize these potential errors, the data was manipulated prior to passing through the tomographic algorithm. Figure 2 illustrates

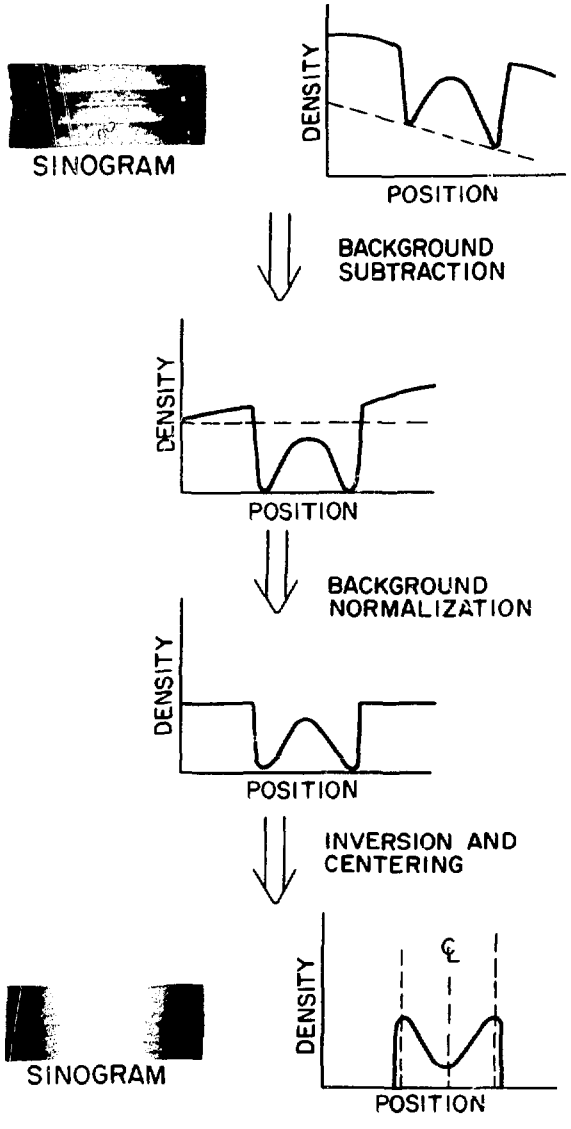


Fig. 2. Projection operations before reconstruction.

the operations performed on each data record (projection). Sinograms of the projections are shown before and after the operations to illustrate the magnitude of these errors. The sinogram shows the individual tomographic projections plotted against the angle of tube rotation.

The axis of rotation was arbitrarily placed midway between the two data minimum. The start of each scan was then defined a fixed distance from the axis of rotation. This operation, while necessary, introduced some error and will be discussed more fully later. The tomographic reconstruction utilized the standard filtered backprojection algorithm[1] and was run on LASL's CDC-7600 computer. The reconstructed image was recorded on a standard digital magnetic tape and was then displayed on a COMTAL 8300 digital display unit.

## III. RESULTS

Figure 3 illustrates the results after some rudimentary image enhancement operations. These operations simply consisted of inverting the gray scale and then expanding a narrow density range in the original data using a linear mapping function on the COMTAL display. Figure 3 also contains a photographic mosaic that maps the features detected in the reconstruction to the features visible to the eye.

## IV. CONCLUSIONS

Figure 3 illustrates the correlation between the visible cracks and the indications detected in the reconstruction. The most important conclusions we can draw at this point are:

1. many of the cracks in the pipe are detected by tomography, and
2. the crack indications visible in the reconstruction appear to have structure (shape and orientation).

The crack images in the reconstruction appear blurred for a number of reasons. First, by not knowing the exact center of rotations of the pipe, the indications are spread out proportional to the uncertainty. Secondly, the cracks do not run perfectly linear along the pipe axis but are somewhat irregular. Since the microdensitometer slit is 1.5 mm long, this in effect integrates along the slit length producing a wider crack image and a lower contrast image. Finally, the finite scanning slit width introduces its own blur factor which must be accounted for. Of these factors, the first two can certainly be reduced. The effect of shortening the slit length will be not only to reduce the integrating effect and hence sharpen the image but also unfortunatly to reduce the signal-to-noise ratio. How far this can be carried before the noise becomes so

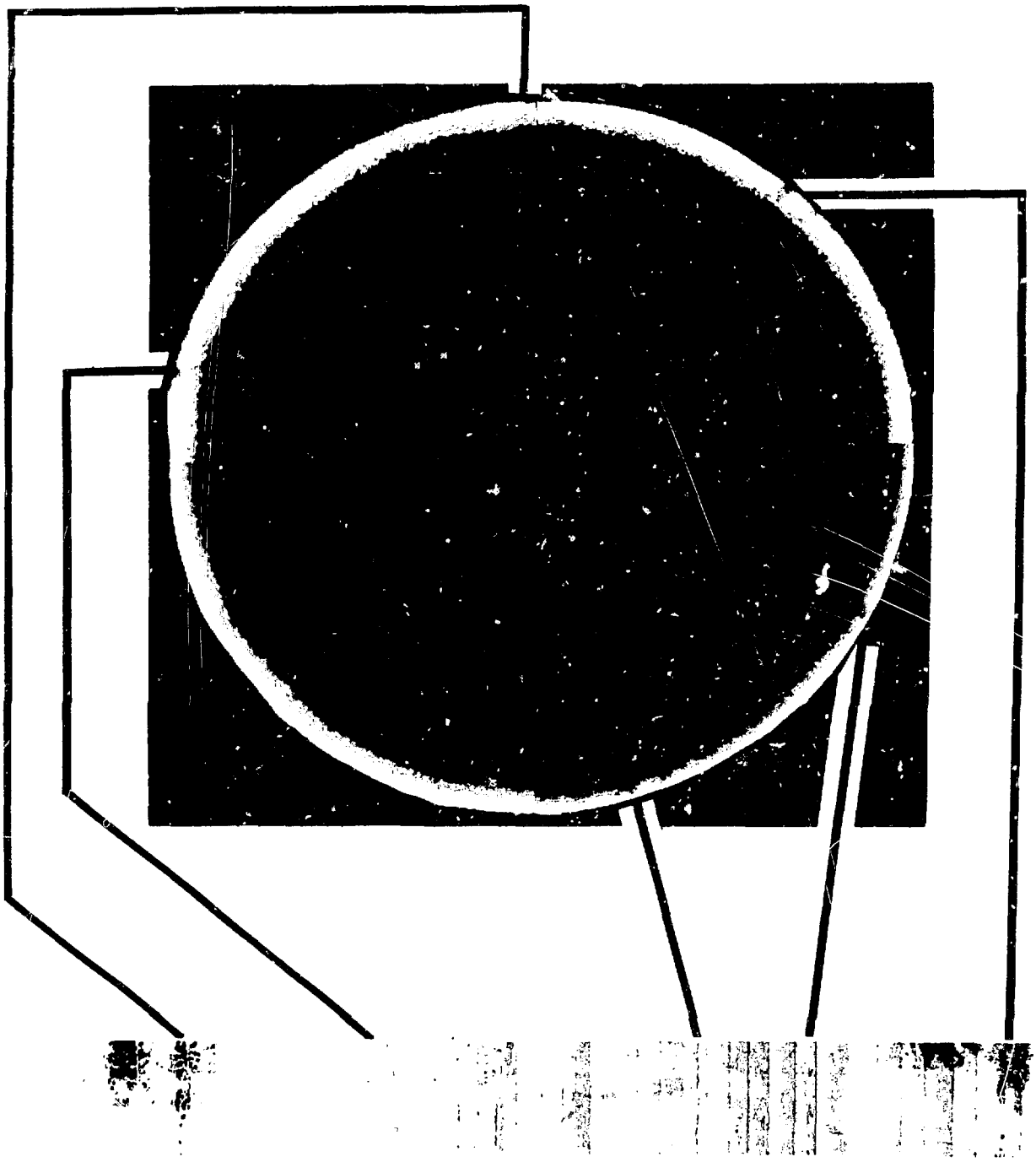

Fig. 3. Tomographic reconstruction of pipe correlated with visible surface indications.

high as to hide defects remains to be studied. Reducing the slit width will have the same effect. Future experiments will use a collimated solid state detector in lieu of film.

We have demonstrated the feasibility of visualizing actual stress corrosion cracks within reactor cooling piping by tomographic reconstruction. We have not determined the spatial resolution of the technique nor explored the functional dependence of spatial resolution with such system parameters as:

1. scanning aperture size,
2. detector resolution (solid state and film),
3. signal-to-noise ratio, and
4. x-ray energy.

The results are highly encouraging and indicate that tomography may become a very important NDE tool when properly developed. The next obvious step to take is to section the pipe in the vicinity of the tomographic section and compare the visual indications with the tomographic indications. At the same time a series of experiments using mock-up and real cracks should be devised to explore the sensitivity of the technique to defect detection.

REFERENCE

1. G. N. Ramachandran and A. V. Lakshminarayauan, "Three Dimensional Reconstruction from Radiographs and Electron Micrographs III. Description and Application of the Convolution Method, "Indian J. Pure Appl. Phys. 9 (1971) 997-1003.

---

## APPENDIX

## FILTERED BACK PROJECTION ALGORITHM

Figure A-1 depicts in symbolic form the scanning and reconstruction process using three projections $p_{\theta j}$ (t) for j = 1, 2, 3. However, the number of projections can vary between 2 and 240 in presently known applications. Each projection value p is essentially a line integral along a path L through the object cross section f relative to an angle $\theta$.

Thus

$$p_\theta(t) = \int_L f(l)dl \qquad (A\text{-}1)$$

for all t and $\theta$. Several such line integrals are symbolized as dotted

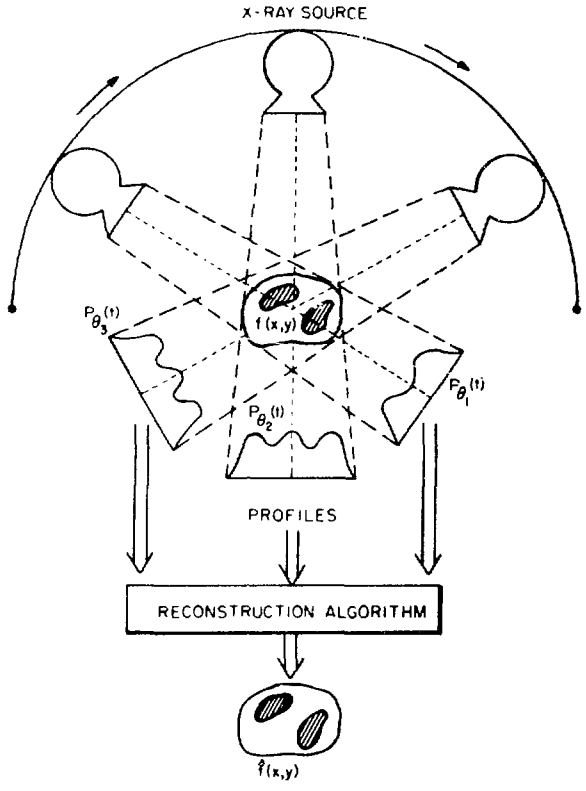


Fig. A-1. Typical tomographic configuration.

lines in Fig. A-1. It has also been shown that source-detector geometry of either the parallel or fan-beam type are equivalent for a judicious choice of projection angles $\Theta$ and thus will not affect the reconstruction process.

Several algorithms have been proposed for accomplishing computed tomography. The algebraic reconstruction techniques (ART) appear to be advantageous when a very limited number of projections are available. However, this application utilized a sufficient number of projections to enable the use of the filtered back projection reconstruction method. The basis of this method will now be discussed. The case where t and $\Theta$ are both continuous will be initially considered.

The one-dimensional Fourier transform of a projection $p_\Theta(t)$ is $\hat{P}_\Theta(v)$ defined

$$\hat{P}_\Theta(v) = \int_{-\infty}^{\infty} p_\Theta(t) e^{-i2\pi vt} dt \qquad (A\text{-}2)$$

where v is measured as a spatial frequency. If $\hat{P}$ is filtered with a frequency domain ramp or rho filter $|v|$ and inverse-transformed, this will produce a filtered projection $\tilde{p}_\Theta(t)$ defined.

$$\tilde{p}_\Theta(t) = \int_{-\infty}^{\infty} \hat{P}_\Theta(v) \, |v| \, e^{i2\pi vt} dv \qquad (A\text{-}3)$$

The rho filter effectively produces the phaseless derivative $\tilde{p}_\Theta(t)$, of the original projection. Using these filtered projections, the cross section $f_z(x,y)$ at a given z-axis height can be reconstructed exactly using

$$f_z(x,y) = \int_0^{\pi} \tilde{P}_\Theta(x \cos\Theta + y \sin\Theta) d\Theta \qquad (A\text{-}4)$$

However, exact reconstruction is not possible since the number of angles $\Theta$ at which projections are actually collected is always discrete and finite.

Also, $p_\Theta(t)$ is usually a sampled or digitized waveform. Thus, for finite $\Theta$ denoted, $\Theta_i$ the reconstruction plane can be approximated by

$$\hat{f}_z(x,y) = \frac{\pi}{K} \sum_{i=1}^{K} \tilde{p}_{\Theta i} (x \cos \Theta_i + y \sin \Theta_i) \quad \text{(A-5)}$$

Where K is the total number of projections. The cross section $\hat{f}_z$ is now an approximation to $f_z$ since $\hat{p}$ and $\Theta_i$ are both discrete and finite. It should also be noted that the x and y indices are now discrete integer picture matrix locations.